Wireless Hydrogen Smart Sensor Based on Pt/Graphene-Immobilized Radio-Frequency Identification Tag

Jun Seop Lee, Jungkyun Oh, Jaemoon Jun, and Jyongsik Jang*

School of Chemical and Biological Engineering, College of Engineering, Seoul National University (SNU), 599 Gwanangno, Gwanak-gu, Seoul 151-742, Korea

ABSTRACT Hydrogen, a clean-burning fuel, is of key importance to various industrial applications, including fuel cells and the aerospace and automotive industries. However, hydrogen gas is odorless, colorless, and highly flammable; thus, appropriate safety protocol implementation and monitoring are essential. Highly sensitive hydrogen-gas leak detection and surveillance systems are needed; additionally, the ability to monitor large areas (*e.g.*, cities) *via* wireless networks is becoming increasingly important. In this report, we introduce a radio frequency identification (RFID)-based wireless smart-sensor system, composed of a Pt-decorated reduced graphene oxide (Pt_rGO)-immobilized RFID sensor tag and an RFID-reader antenna-connected network analyzer to detect hydrogen gas. The Pt_rGOs, produced using a simple chemical reduction process, were immobilized on an antenna pattern in the sensor tag through spin coating. The resulting Pt_rGO-based RFID sensor tag exhibited a high sensitivity to hydrogen gas at unprecedentedly low concentrations (1 ppm), with wireless communication between the sensor tag and RFID-reader antenna. The wireless sensor tag demonstrated flexibility and a long lifetime due to the strong immobilization of Pt_rGOs on the substrate and battery-independent operation during hydrogen sensing, respectively.

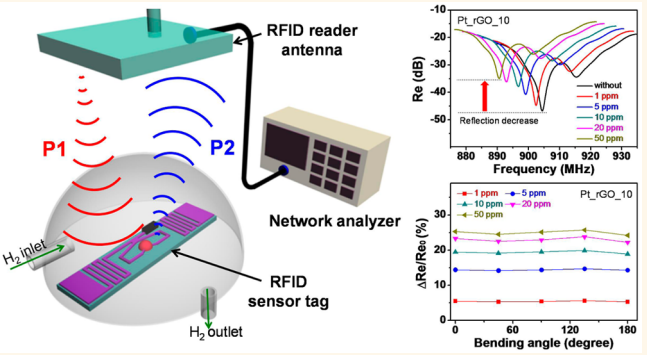

KEYWORDS: hydrogen · graphene · wireless sensor · platinum · flexible

The sensing ability of hazardous and flammable substances in the environment has received much attention due to the demands of various application fields, such as disaster prevention, home automation, healthcare, and advanced traceability systems.[1−5] Sensor devices based on nanoscale materials offer unprecedented sensing transducer opportunities owing to their high sensitivity to targeted analytes originated from their small size (*i.e.*, high surface-to-volume ratio).[6−10] Despite the incredible potential of nanoscale sensors, mass production has been limited by the difficulty in integrating the sensor components into electronic circuits. Several approaches have been investigated in an attempt to improve integration.[11−15] Among the various approaches, the integration of nanoscale sensors into wireless communication networks is of particular interest because of the nonobtrusive nature of the installation, high nodal densities, and low installation costs (without the need for extensive wiring).[16−18] These attractive features of wireless sensors facilitate their use in measurements over a wide range of applications, including monitoring of analyte gases (carbon dioxide, water vapor, oxygen, and flammables) in relatively interference-free industrial and indoor environments, in addition to wearable sensors in the workplace, in urban environments, and for military personnel.[19−21]

One of wireless smart-sensing systems, the radio frequency identification (RFID)-based sensor has emerged as a promising device on account of its simple architecture and broad detection range of target analytes.[22−26] An RFID-based wireless sensor system can be operated using only two components, the sensor tag (*i.e.*, signal transfer) and interrogation reader (*i.e.*, signal receiver), without the need for additional equipment. As a signal transfer device, sensor tags can be classified into two types: (1) battery-operated

* Address correspondence to jsjang@plaza.snu.ac.kr.

Received for review April 4, 2015 and accepted June 10, 2015.

Published online June 10, 2015
10.1021/acsnano.5b02024

sensor tags (active) and (2) sensor tags that do not require a battery (passive). Among the two types, passive sensor tags show great potential due to their longer lifetime, smaller size, and cost-effectiveness compared with active tags.[27,28] Additionally, passive sensor tags transfer signals to the reader using a zero-power backscatter communication process.[29] However, passive sensor tags have a shorter detection range than active sensor tags.[27,29] Recently, a passive ultrahigh frequency (UHF) RFID sensor tag has been applied to wireless sensor systems to enhance the sensing range distance and signal strength.[30−32]

Hydrogen gas is widely used in industrial applications, including fossil-fuel production, chemical compound synthesis, power plant operation, fuel-cell applications, and in the aerospace and automotive industries.[33−36] In recent years, hydrogen energy has received a great deal of attention for next-generation applications, such as hydrogen-based zero-carbon emission vehicles.[37−39] However, because of the wide explosive range of hydrogen (4−75 vol %), safe storage is a critical issue when working with gases containing hydrogen.[40,41] Thus, rapidly responsive sensors are necessary to monitor hydrogen levels. Moreover, the demand also increases for wireless hydrogen-sensing surveillance systems with city-scale capabilities.

Herein, we report the fabrication of a flexible RFID-based wireless smart sensor to detect hydrogen gas at room temperature. The wireless smart sensor is composed of two components: an RFID antenna-connected network analyzer as an interrogation reader and a platinum (Pt)-decorated reduced graphene oxide (Pt_rGO) immobilized passive UHF-RFID tag as a sensing tag. Owing to the large surface area of the two-dimensional (2-D) graphene sheet morphology, the Pt_rGOs easily formed a hydrogen-sensing area on the antenna pattern of the RFID sensor tag through spin coating. During hydrogen detection, the decorated Pt particles on the rGO surface created a strong affinity between Pt and hydrogen gas, as indicated by the change in resistivity of the antenna, resulting in a shift in the reflectance of the RFID sensor tag. The RFID-based wireless sensor displayed a significant reflectance shift with varying hydrogen gas concentration and exhibited recognition at unprecedentedly low concentrations (1 ppm). Additionally, this wireless smart sensor showed flexibility under deformation as well as a long lifetime on account of the strong immobilization of Pt_rGOs on the substrate and the battery-independent operation of the sensor tag.

RESULTS AND DISCUSSION

An overview of ultrahigh frequency (UHF) RFID-based wireless sensing system for detect hydrogen gas is suggested in Figure 1. The system consisted of an RFID-reader antenna-connected interrogating network analyzer and a sensing material immobilized

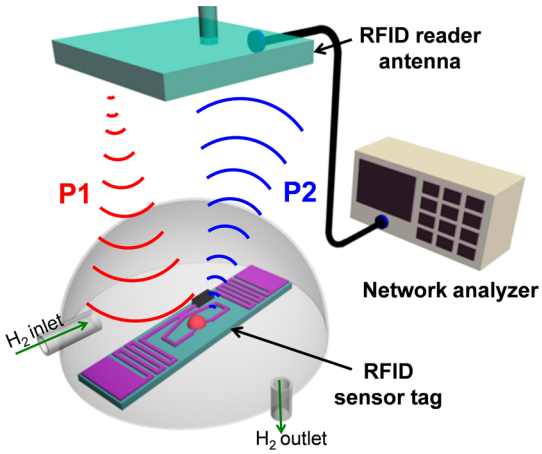

Figure 1. Schematic diagram of the ultrahigh frequency (UHF)-RFID-based wireless sensor system composed of an RFID sensor tag and RFID-antenna-connected network analyzer.

UHF-RFID sensor tag that included the dipole tag antenna, sensing area, and IC chip. The wireless sensing system based passive RFID tag network is described as follows. The network analyzer emitted an interrogation signal at a power threshold of P1 to activate the sensor tag when the sensor tag is in the RFID-reader antenna's electromagnetic field. The signal was then reflected back to the RFID-reader antenna at a power level of P2 (that is called backscattering) based on its radar cross section.[23,30] According to the impedance matching between the dipole tag antenna and the IC chip of sensor tag, the reflected signal morphology (*i.e.*, amplitude and phase) of sensor tag changed with different surroundings, that is, detection of target analyte at the sensing area. As a result, the wireless hydrogen sensing occurred through this backscattering sequence between the RFID sensor tag and the RFID-reader antenna.

As a sensing material, platinum-decorated reduced graphene oxide (Pt_rGO) was fabricated as in the following steps (Supporting Information Figure S1). In the first step, a graphene oxide (GO) aqueous solution, as the starting material, was synthesized using the modified Hummers and Offman method. Different concentrations (0.1−10 mmol) of $PtCl_4$ aqueous solutions were mixed with the GO solution to induce charge−charge interaction between the partial negative charge of the oxygen atom in the GO structure and the positive charge of Pt cations.[42,43] Once the Pt cations adsorbed to the GO surface, a small amount of $NaBH_4$ was introduced to reduce the Pt cations from Pt^{4+} to Pt^0. Consequently, a Pt-decorated GO sheet (Pt_GO) was created. Then, hydrazine ($N_2H_4 \cdot H_2O$) was added to the Pt_GO solution under vigorous stirring to convert the GO sheet to reduced-GO (rGO). The resulting Pt-decorated rGO (Pt_rGO) exhibited *ca.* 5 nm-diameter Pt particles on its surface. The amount of Pt-particle decoration increased with the $PtCl_4$ solution concentration, as shown in Figure 2a−c; Pt_rGO nanocomposites with different $PtCl_4$ concentrations of 0.1, 1,

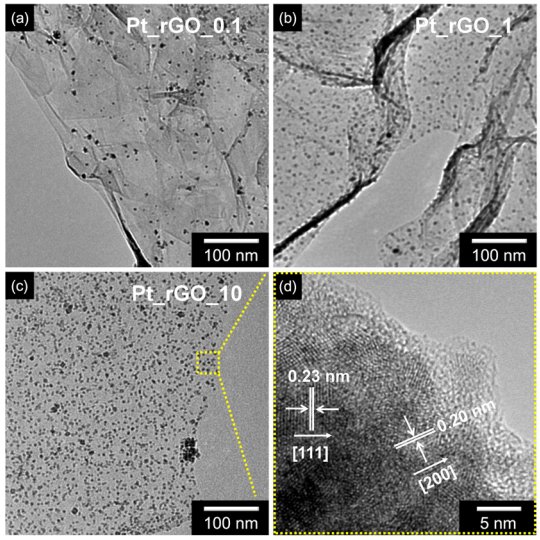

Figure 2. Transmission electron microscopy (TEM) images of Pt-decorated reduced graphene oxide (Pt-rGO) for different concentrations of $PtCl_4$ aqueous solution (0.1, 1, and 10 mmol mixed with GO, denoted as Pt_rGO_0.1, Pt_rGO_1, and Pt_rGO_10, respectively): (a) Pt_rGO_0.1, (b) Pt_rGO_1, and (c) Pt_rGO_10. (d) High-resolution TEM (HR-TEM) image of Pt_rGO_10.

and 10 mmol are denoted as Pt_rGO_0.1, Pt_rGO_1, and Pt_rGO_10, respectively. High-resolution transmission electron microscopy (HR-TEM) indicated an interplanar spacing between the metal particles of 0.23 and 0.20 nm for the (111) and (200) planes, respectively, corresponding to the face-centered cubic (fcc)-Pt lattice structure (Figure 2d). Furthermore, Raman and X-ray diffraction (XRD) spectra of each composite confirmed Pt-particle decoration of the rGO surface during the chemical reduction process (Supporting Information Figure S2).

To characterize the electrical properties of the Pt_rGO, an interdigitated microelectrode array (IDA)-based chemical-sensing configuration was fabricated *via* spin coating. Supporting Information Figure S3 displays uniformly dispersed Pt_rGO on the IDA electrode composed of 2-μm-width gold fingers, totaling 40 fingers. Current−voltage ($I-V$) curves were used to evaluate the electrical conductivity and contact type of the uniformly decorated Pt_rGOs on the IDA substrate for various Pt nanoparticle decoration amounts (Figure 3a). Each Pt_rGO sample suggested linearity (*i.e.*, ohmic contact) over the voltage range from −0.1 to 0.1 V, as opposed to the nonlinearity presented by Schottky barriers with poor electrical contact at the electrode. The dI/dV values of the electrodes increased with the amount of Pt nanoparticles on the rGO surface; this was attributed to the enhanced conductivity of the rGO sheets owing to the Pt particles.

The uniformly dispersed Pt_rGO on the sensor substrate rapidly detected hydrogen gas at room temperature. The sensing mechanism of the Pt_rGO is described below (Supporting Information Figure S4).[38,39] Initially, the hydrogen gas molecules adsorb to the Pt particles on the rGO sheet. The hydrogen molecules then dissociate and form two H atoms through the catalytic properties of the Pt particles. The two H atoms react with the Pt particles to form the complex hybrid, PtH_x. The electrons generated move to the graphene sheets due to the lower work function of PtH_x compared with that of rGO. The transferred electrons decrease the number of holes in the rGO and increase its electrical resistance (*i.e.*, rGO acts as a *p*-type transducer).[4,44] Thus, the Pt particles play a key role in hydrogen gas detection in the sensing mechanism. In the sensing mechanism, the Pt particles first bond to the hydrogen gas molecules *via* a chemisorption interaction. The number of hydrogen-sensing active sites increases with the concentration of Pt particles decorating on the rGO surface.

The real time response of various Pt_rGO composites on the IDA electrode was measured for different concentrations of hydrogen gas (Figure 3b). In the pristine rGO case, sensitivity to the hydrogen gas was absent because no functional sites were available to attract the hydrogen molecules. In contrast, when the Pt_rGO-based sensors were exposed to hydrogen gas at room temperature, excellent sensitivity and rapid response/recovery times were observed (Supporting Information Figure S5 and Table S1). The sensitivity of Pt_rGO increased with the size and density of Pt particles on the surface. Pt_rGO_10, in particular, detected hydrogen concentrations as low as 1 ppm at room temperature. Figure 3c shows the electrical response of various Pt_rGOs upon periodic exposure to 50 ppm of hydrogen gas at room temperature. With the exception of pristine rGO, these nanocomposites revealed similar response sensitivities with enhanced sensing number, without retardation of the response or recovery times. The sensitivity S, defined as the normalized resistance change measured after a 15-s gas exposure, was measured as a function of the gas concentration (Figure 3d). At low concentrations (<1 ppm), the Pt_rGO sensors exhibited a nonlinear change in their sensitivity. In contrast, linear behavior was observed over a wide range of concentrations (1−100 ppm). Thus, the Pt_rGO-based IDA electrode gas sensors demonstrated reversible, reproducible responses to different hydrogen concentrations, and their responses were more pronounced as the gas concentration increased.

To enable wireless sensor application, the as-prepared Pt_rGO nanocomposites were immobilized on the antenna pattern of the passive UHF (*ca.* 900 MHz)-RFID tag by spin coating (Figure 4a). The used passive UHF-RFID tag consisting of a micropatterned dipole-tag antenna on a plastic substrate, with an interdigitated circuit (IC) chip located in the middle of the antenna. To fabricate wireless sensor tag, the sensing area in the RFID tag was fabricated by first covering the RFID tag with plastic tape, with the exception of a 3 × 6 mm area of the antenna pattern. The Pt_rGO solution was then deposited onto the sensing area by drop casting. The Pt_rGO-solution-deposited RFID tag was spin-coated at

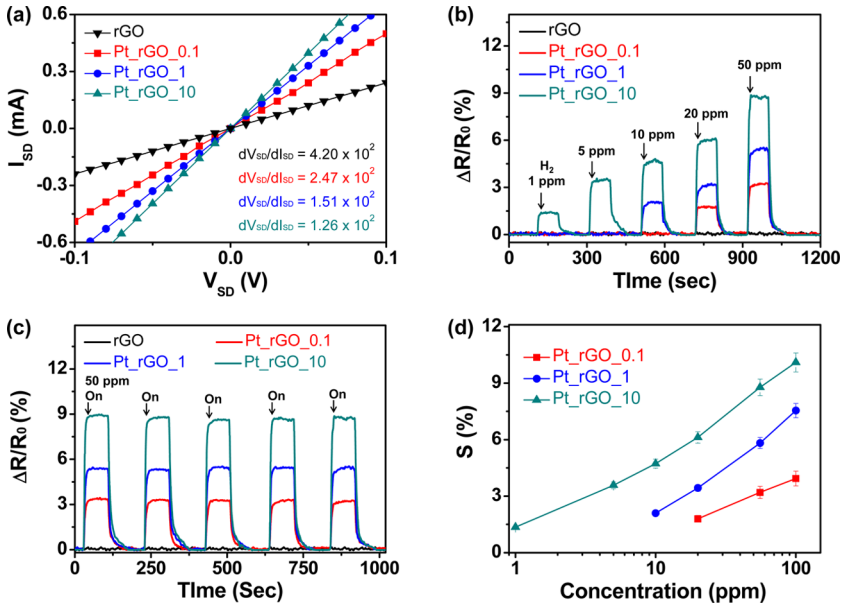

Figure 3. (a) Current−voltage (*I*−*V*) curves for the interdigitated array (IDA) electrodes based on different Pt particles on the rGO surface (black, rGO; red, Pt_rGO_0.1; blue, Pt_rGO_1; green, Pt_rGO_10). Reversible and reproducible responses were measured at constant current value (10^{-6} A). Normalized resistance changes upon sequential exposure to (b) various concentrations of hydrogen gas and (c) periodic exposure to 50-ppm hydrogen gas. (d) Calibration curves of Pt_rGOs as a function of hydrogen gas concentration (black, rGO; red, Pt_rGO_0.1; blue, Pt_rGO_1; green, Pt_rGO_10).

1000 rpm for 45 s to uniformly immobilize the Pt_rGOs on the sensing area, resulting in an RFID-based wireless hydrogen sensor tag, as shown in the Supporting Information Figure S6. Enlarged optical microscopy and field effect scanning electron microscopy (FE-SEM) images of the hydrogen-sensing area revealed that the Pt_rGOs were well dispersed over the antenna pattern without aggregation (Figure 4b−d). The highly uniform immobilization was attributed to the strong adsorption to the substrate resulting from the large surface area of the 2-D graphene structures.[45] Additionally, the Pt_rGO-immobilized RFID sensor tag exhibited mechanical stability with bending and twisting deformations owing to the flexibility of the plastic sensor substrate and strong adsorption of Pt_rGOs on the metal substrate (Figure 4e).

The as prepared sensor tags were applied to UHF (*ca.* 900 MHz) RFID-based wireless hydrogen gas sensing system. Figure 5a−c displays the change in the reflection amount radio frequency of the different sensor tags (Pt_rGO_0.1, Pt_rGO_1, and Pt_rGO_10, respectively) under a 2 min exposure to various concentrations of hydrogen gas at room temperature, at a distance of 10 cm. The reflection signals were plotted as power of the radio waves reflected (Re, in dB) *versus* the frequency (MHz), as determined by the network analyzer. The RFID sensor tags without hydrogen exposing displayed larger reflection than others owing to outstanding impedance matching between antenna and IC chip. However, when the sensor tag is exposed to hydrogen gas, the hydrogen gas adsorbs to the Pt particles and then electrons transfer to the rGO, increasing the resistivity of the antenna with an enhancement in the hydrogen gas concentration (the resistance of the tags increased from 3.2 to 16.1 Ω with an increase in the hydrogen gas concentration (1−50 ppm)). The increasing resistance of tag antenna leads to impedance mismatching of between antenna and IC chip compared to without hydrogen exposure and then, the RFID sensor tag decreases radar cross section resulting in a diminish reflection.[27] Furthermore, similar to the IDA-based sensing system, the sensitivity of the wireless hydrogen sensor increased with the Pt-particle concentration (1 ppm for Pt_rGO_10; 10 ppm for Pt_rGO_1; 20 ppm for Pt_rGO_0.1). Additionally, the measured reflection phase shifts of the sensor tags are suggested as shown in the Figure 5d−f. The phase shift amount of sensor tag also increases with enhanced exposure of hydrogen concentration and population Pt particles in the rGO surface as the same mechanism in the reflection case.

Figure 5g shows the wireless sensor response calibration (normalized reflection change) as a function of the hydrogen gas concentration; the normalized reflection change is expressed as $(Re - Re_0)/Re_0$ $(= \Delta Re/Re_0)$, where Re is the reflection after 2 min of hydrogen exposure and Re_0 is the reflectance at the beginning of the experiment. The normalized reflection of the radio waves increased with the hydrogen gas concentration for all sensor tag samples. Additionally, the reflection difference (%) increased with the concentration of Pt particles on rGO (21.4% for Pt_rGO_10; 8.4% for Pt_rGO_1; 5.2% for Pt_rGO_0.1 at 20 ppm of hydrogen). However, the change amount of reflection decreased with increasing concentrations more than a 50 ppm level, indicating a trend toward saturation of the sensor tag with hydrogen gas. In addition, calibrated reflection phases also suggest decreasing frequency

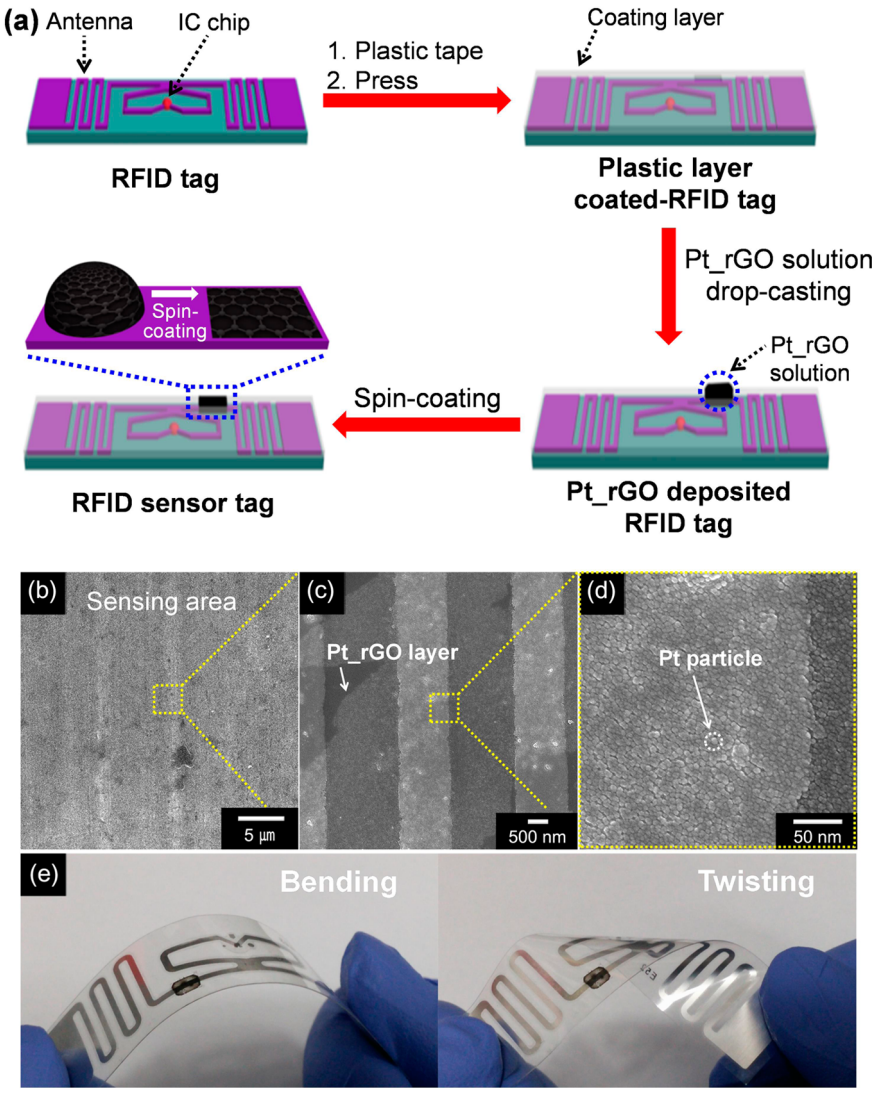

Figure 4. (a) Schematic diagram of a Pt_rGO-immobilized radio frequency identification (RFID) sensor tag. Field effect scanning electron microscopy (FE-SEM) (b) low-, (c) middle-, and (d) high-resolution images of the Pt_rGO immobilized sensing area. (e) Photographs of the RFID sensor tag under different deformations (bending and twisting).

with increasing hydrogen gas concentration and exhibit saturation over 50 ppm at room temperature (Figure 5h).

Furthermore, reflection changes of wireless sensors with different remote distance (from 5 to 25 cm) are shown in the Supporting Information Figure S7. Due to reducing backscattering effect with enhancement remote distance, the reflection change decreased as the distance between sensor electrode and RFID reader antenna increased. In addition, there is no significant reflection peak above 25 cm because of absence of backscattering effect. Additionally, Figure 5i presents the average change in reflection of the Pt_rGO_10 UHF-RFID-based sensor tag through various folding angles. The folding angle is bending degree of substrate with compressive force as shown in Supporting Information Figure S8. It also related with folding angles that smaller bending radius caused greater folding angle as the radius of curvature decreases. Therefore, folding angles of RFID sensor tag was controlled through manipulating bending radius as shown in Supporting Information Figure S9. No significant difference was observed during the application of repetitive bending deformations owing to the uniformity of the sensor tag components on the substrate. Thus, the proposed Pt_rGO-based RFID sensor is applicable to real life use as a wearable or implantable wireless-sensing system.

Therefore, there are several superb characteristics of this RFID-based wireless sensing systems over other nanoscale palladium-based resistive hydrogen sensors.[46,47] Most of all, this sensing system conducted through wireless communication system with radio frequency wave between signal transfer (RFID sensor tag) and receiver (RFID antenna) and exhibited distinct characteristics such as nonobtrusive nature of installation, high nodal densities, and low installation costs (without the need for extensive wiring). In addition, passive type RFID-tag based sensor electrodes, without energy generating device in the tag, operated

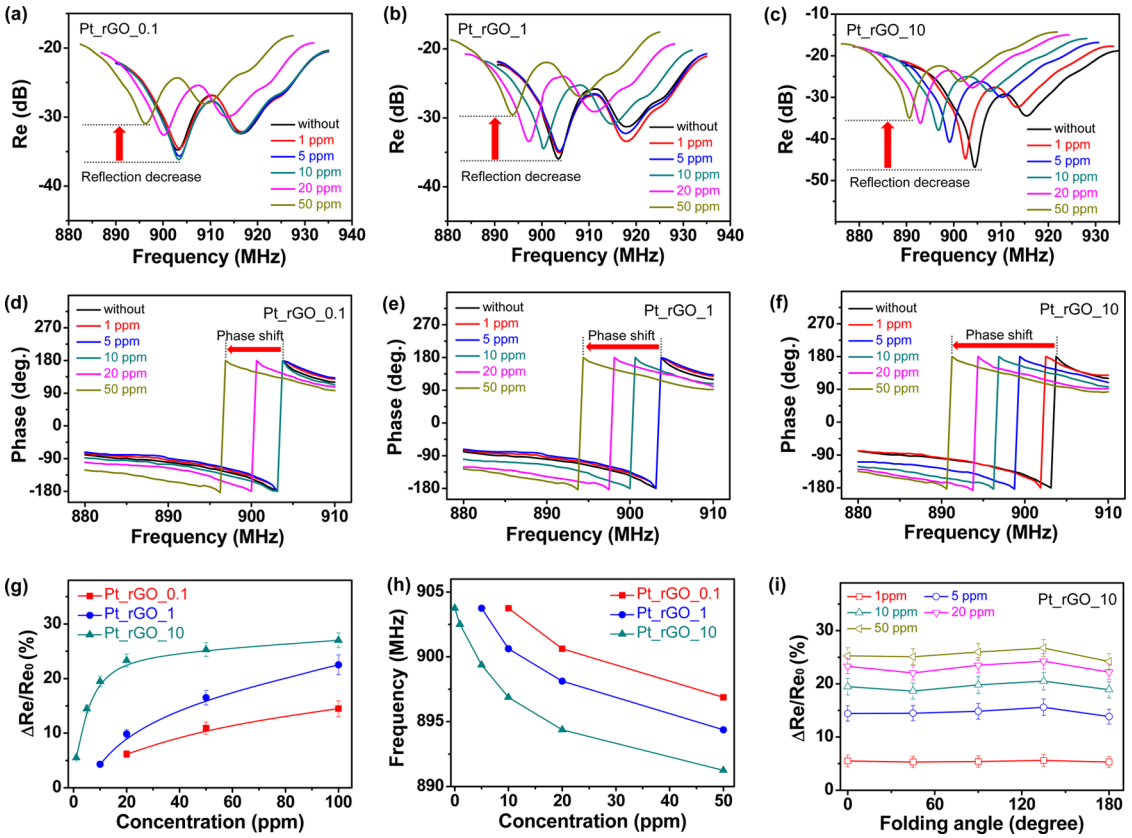

Figure 5. Change in the reflectance properties and measured reflection phase of different Pt_rGOs-based wireless sensors as a function of the hydrogen gas concentration for a 2 min exposure (distance, 10 cm): (a and d) Pt_rGO_0.1; (b and e) Pt_rGO_1; (c and f) Pt_rGO_10 (black, without hydrogen gas; red, 1 ppm; blue, 5 ppm; green, 10 ppm; pink, 20 ppm; yellow, 50 ppm). (g) Reflection calibration curves of the three wireless sensor tags as a function of hydrogen concentration ($\Delta Re/Re_0 = (Re - Re_0)/Re_0$, where Re_0 is the initial reflectance and Re is the reflectance after a 2 min exposure). (h) Phase shift calibration curves of the three wireless sensor tags as a function of hydrogen concentration. Red, blue, and green represent wireless sensor tags originating from Pt_rGO_0.1, Pt_rGO_1, and Pt_rGO_10, respectively. (i) Average reflectance curves of a Pt_rGO_10-based wireless sensor tag as a function of the sensor tag folding angles at 10 cm with different hydrogen gas concentrations (red, 1 ppm; blue, 5 ppm; green, 10 ppm; pink, 20 ppm; yellow, 50 ppm).

permanently by external energy source stimulus. Moreover, Pt_rGO also displayed superb characteristics to apply sensing material of RFID tag-based sensor electrode. First, Pt_rGO easily formed sensing area on the antenna pattern of RFID tag and showed structure stability during deformations on account of strong physisorption originated from large surface area of 2-dimensional graphene sheet morphology. Second, the Pt_rGO revealed high sensitivity to hydrogen gas and stable cycle stability owing to enlarged surface area came from uniformly decorated Pt particles on the rGO surface.

CONCLUSION

In summary, we fabricated an RFID-based wireless smart-sensor system consisting of a Pt_rGO-immobilized RFID sensor tag and an RFID-reader antenna-connected network analyzer. Pt_rGOs were immobilized on the antenna micropattern in the sensor tag *via* spin coating, taking advantage of the physisorption between the Pt_rGO and the antenna. The Pt_rGO RFID sensor tag exhibited high sensitivity (1 ppm) to hydrogen gas and uniform sensing ability under bending deformations because of strong bonding between Pt_rGO and the substrate. Additionally, the Pt-rGO sensor tag operated without a battery during backscattering communication, promoting a long lifetime for the sensor tag. Thus, this study demonstrated a highly sensitive, flexible, wireless smart sensor for hydrogen detection *via* immobilization of noble-metal-decorated graphene composites in the RFID sensor tag.

MATERIALS AND METHODS

Fabrication of Pt_rGO Nanocomposites. Graphene oxide (GO) was obtained from graphite flake (99%, Aldrich) using the modified Hummers and Offman method. The as-prepared GO was dispersed in an aqueous solution at 0.25 wt %. $PtCl_4$ (99%, Kojima Chemical), in the amount of 0.1, 1.0, and 10 mmol, was added to the GO aqueous solution. The mixed solution was introduced to 1 mmol of $NaBH_4$ as a reducing agent and then stirred for 1 h at 25 °C. The Pt-decorated GO (Pt_GO) solution was then reduced by adding $N_2H_4 \cdot H_2O$ (1/1000 v/v *vs* distilled water) under vigorous stirring at 95 °C for 1 h. The prepared Pt-particle-decorated reduced GO (Pt_rGO) solution was filtered using

excess distilled water and ethanol. Powders of Pt_rGO were obtained through drying in a vacuum oven at 25 °C for 24 h.

Electrical Measurement of the Pt_rGO on the IDA Electrode. The electrical measurements of the Pt_rGOs were measured using an interdigitated array (IDA) electrode. The Pt_rGOs (0.1 wt % in ethanol solution) were prepared by sonication for deposition on the as-prepared IDA. The samples were introduced by the drop-casting method to the IDA surface to reduce the contact resistance between the particles. In the droplet process, a spin-coating method (1000 rpm, 45 s) was used to produce a uniform array. The physical adsorption of Pt_rGOs on the substrate was followed by drying at 25 °C in an inert atmosphere for 1 h to obtain good electrical ohmic contact between the Pt_rGO and electrode. Resistance changes in the Pt_rGO were monitored with a source meter connected to a computer. The Pt_rGO IDA electrodes were placed in a vacuum chamber having a vapor inlet/outlet pressure of 10° Torr. Various H_2 gas concentrations (1−100 ppm) were introduced into the chamber by a mass flow controller (MFC, KNH Instruments). The real-time resistance was monitored at a constant applied current of 10^{-6} A (defined as $\Delta R/R_0 = (R - R_0)/R_0$, where R and R_0 are the real-time and initial resistances, respectively). After the Pt_rGO interacted with different concentrations of H_2 gas for several minutes, each vapor was replaced by compressed air to remove the molecules attached to the backbone of the Pt_rGOs; this process was repeated several times. Vapor/air was supplied at various flow rates of 2−8 slm and 1−5 sccm using the MFC.

Fabrication of the Pt_rGO-Based Wireless Smart-Sensor System. To fabricate the RFID sensor tag, one component of the RFID-based wireless sensor system, the passive UHF-RFID tag (nominal frequency: *ca.* 904 MHz (EMPO Corp.)) was covered with plastic tape, with the exception of a 3 × 6 mm^2 area on the antenna pattern. The passive UHF-RFID tag consisted of an antenna and microcontroller integrated circuit (IC) chip (EPC Global Class-1 Generation-2 (Gen2) protocol) on a flexible plastic substrate. Additionally, the UHF-RFID tags are $2 U.S. dollars by the piece. A total of 50 μL of the prepared Pt_rGO solutions (0.1 wt % in ethanol) was deposited through drop casting onto the exposed antenna pattern area. The Pt_rGO solution-deposited RFID tag was then spin-coated at 1000 rpm for 45 s to create uniform coverage of the immobilized Pt_rGOs over the controlled area.

The RFID reader apparatus was constructed from the RFID reader antenna (ThingMagic Corp., cost: $1500 U.S. dollars). The frequency range of the reader antenna was 865−956 MHz. The antenna was connected to a network analyzer (E5071B, Agilent Technologies, cost: $40 000 U.S. dollars).

Electrical Measurement of the Pt_rGO-Based Wireless Smart Sensor. The as-prepared wireless sensor tag was placed in a vacuum chamber for exposure to various concentrations of hydrogen gas (H_2) (range: 1−100 ppm) by the MFC (KNH Instruments). The wireless sensor response corresponded to backscattering measurements between the sensor tag and the RFID reader antenna connected to the network analyzer. The network analyzer scanned the frequencies over the range of interest and collected the complex impedance response from the sensor tag. The RFID reader antenna was positioned at different distances from the chamber, and each tag was read individually. The collected complex impedance data were analyzed using KaleidaGraph (Synergy Software, Reading, PA) and PLS_Toolbox (Eigenvector Research Co.) operated with Matlab (The Mathworks, Inc.). The resistance of the RFID tags was measured with a digital multimeter (Mastercraft, Inc.).

Instruments. Transmission electron microscopy (TEM) and high-resolution TEM (HR-TEM) images were obtained with JEOL JEM-200CX and JEOL JEM-3010 microscopes, respectively. A JEOL 6700 instrument was used to obtain field-effect scanning electron microscopy (FE-SEM) images. X-ray diffraction (XRD) and Raman spectra were recorded using M18XHF SRA (MAC Science Co.) and T64000 (HORIABA Jobin Yvon) systems, respectively.

Conflict of Interest: The authors declare no competing financial interest.

Supporting Information Available: The contents of the Supporting Information include the following: (1) fabrication steps of Pt_rGO; (2) characterization of Pt_rGO; (3) deposition of Pt_rGO on the IDA electrode; (4) sensing mechanism of hydrogen gas; (5) response and recovery times of Pt_rGO based IDA sensor electrode; (6) hydrogen gas detection comparison of Pt_rGO based IDA sensor electrode; (7) real image of RFID sensor tag; (8) wireless sensing ability with different remote distances; (9) definition of folding angle; (10) diverse folding angles of RFID sensor electrode. The Supporting Information is available free of charge on the ACS Publications website at DOI: 10.1021/acsnano.5b02024.

Acknowledgment. This research was supported by the National Research Foundation of Korea (NRF) grant funded by the Korea government (MEST) (No. 2011-0017125)

REFERENCES AND NOTES

1. Gao, W.; Wang, J. The Environmental Impact of Micro/Nanomachines: A Review. *ACS Nano* **2014**, *8*, 3170–3180.
2. Lee, J. S.; Kwon, O. S.; Shin, D. H.; Jang, J. WO_3 Nanonodule-Decorated Hybrid Carbon Nanofibers for NO_2 Gas Sensor Application. *J. Mater. Chem. A* **2013**, *1*, 9099–9106.
3. She, G.; Huang, X.; Jin, L.; Qi, Z.; Mu, L.; Shi, W. SnO_2 Nanoparticle-Coated ZnO Nanotube Arrays for High-Performance Electrochemical Sensors. *Small* **2014**, *10*, 4685–4692.
4. Ni, H.; Wang, M.; Shen, T.; Zhou, J. Self-Assembled Large-Area Annular Cavity Arrays with Tunable Cylindrical Surface Plasmons for Sensing. *ACS Nano* **2015**, *9*, 1913–1925.
5. Lee, J. S.; Shin, D. H.; Jun, J.; Jang, J. Multidimensional Polypyrrole/Iron Oxyhydroxide Hybrid Nanoparticles for Chemical Nerve Gas Agent Sensing Application. *ACS Nano* **2013**, *7*, 10139–10147.
6. Jang, J. Conducting Polymer Nanomaterials and Their Applications. *Adv. Polym. Sci.* **2006**, *199*, 189–259.
7. Zhan, B.; Li, C.; Yang, J.; Jenkins, G.; Huang, W.; Dong, X. Graphene Field-Effect Transistor and Its Application for Electronic Sensing. *Small* **2014**, *10*, 4042–4065.
8. Chapman, R.; Lin, Y.; Burnapp, M.; Bentham, A.; Hillier, D.; Zabron, A.; Khan, S.; Tyreman, M.; Stevens, M. M. Multivalent Nanoparticle Networks Enable Point-of-Care Detection of Human Phospholipase-A2 in Serum. *ACS Nano* **2015**, *9*, 2565–2573.
9. Lee, J. S.; Jun, J.; Shin, D. H.; Jang, J. Urchin-Like Polypyrrole Nanoparticles for Highly Sensitive and Selective Chemiresistive Sensor Application. *Nanoscale* **2014**, *6*, 4188–4194.
10. Jiang, R.; Qin, F.; Ruan, Q.; Wang, J.; Jin, C. Ultrasensitive Plasmonic Response of Bimetallic Au/Pd Nanostructures to Hydrogen. *Adv. Funct. Mater.* **2014**, *24*, 7328–7337.
11. Cui, Y.; Wei, Q.; Park, H.; Lieber, C. M. Nanowire Nanosensors for Highly Sensitive and Selective Detection of Biological and Chemical Species. *Science* **2001**, *293*, 1289–1292.
12. Zang, Y.; Zhang, F.; Huang, D.; Di, C.-A.; Meng, Q.; Gao, X.; Zhu, D. Specific and Reproducible Gas Sensors Utilizing Gas-Phase Chemical Reaction on Organic Transistors. *Adv. Mater.* **2014**, *26*, 2862–2867.
13. Lin, Y.; Lu, F.; Tu, Y.; Ren, Z. Glucose Biosensors Based on Carbon Nanotube Nanoelectrode Ensembles. *Nano Lett.* **2004**, *4*, 191–195.
14. Lee, J. S.; Kwon, O. S.; Park, S. J.; Park, E. Y.; You, S. A.; Yoon, H.; Jang, J. Fabrication of Ultrafine Metal-Oxide-Decorated Carbon Nanofibers for DMMP Sensor Application. *ACS Nano* **2011**, *5*, 7992–8001.
15. Wang, S.; Mu, X.; Yang, Y.; Sun, C.; Gu, A. Y.; Wang, Z. L. Flow-Driven Triboelectric Generator for Directly Powering a Wireless Sensor Node. *Adv. Mater.* **2015**, *27*, 240–248.
16. Hu, Y.; Zhang, Y.; Xu, C.; Lin, L.; Snyder, R. L.; Wang, Z. L. Self-Powered System with Wireless Data Transmission. *Nano Lett.* **2011**, *11*, 2572–2577.
17. Jeon, J.; Lee, H.-B.-R.; Bao, Z. Flexible Wireless Temperature Sensors Based on Ni Microparticle-Filled Binary Polymer Composites. *Adv. Mater.* **2013**, *25*, 850–855.
18. Chen, L. Y.; Tee, B. C-K.; Chortos, A. L.; Schwartz, G.; Tse, V.; Lipomi, D. J.; Wong, H-S. P.; McConnell, M. V.; Bao, Z. Continuous Wireless Pressure Monitoring and Mapping

with Ultra-Small Passive Sensors for Health Monitoring and Critical Care. *Nat. Commun.* **2014**, *5*, 5028–5037.
19. Byrne, R.; Diamond, D. Chemo/Bio-Sensor Networks. *Nat. Mater.* **2006**, *5*, 421–424.
20. Diamond, D.; Coyle, S.; Scarmagnani, S.; Hayes, J. Wireless Sensor Networks and Chemo-/Biosensing. *Chem. Rev.* **2008**, *108*, 652–679.
21. Espinosa, E.; Ionescu, R.; Zampolli, S.; Elmi, I.; Cardinali, G. C.; Abad, E.; Leghrib, R.; Ramirez, J. L.; Vilanova, X.; Llobet, E. Drop-Coated Sensing Layers on Ultra Low Power Hotplates for an RFID Flexible Tag Microlab. *Sens. Actuators, B* **2010**, *144*, 462–466.
22. Donno, D. D.; Catarinucci, L.; Tarricone, L. A Battery-Assisted Sensor-Enhanced RFID Tag Enabling Heterogeneous Wireless Sensor Networks. *IEEE Sens. J.* **2014**, *14*, 1048–1055.
23. Vyas, R.; Lakafosis, V.; Lee, H.; Shaker, G.; Yang, L.; Orecchini, G.; Traille, A.; Tentzeris, M. M.; Roselli, L. Inkjet Printed, Self Powered, Wireless Sensors for Environmental, Gas, and Authentication-Based Sensing. *IEEE Sens. J.* **2011**, *11*, 3139–3152.
24. Fiddes, L. K.; Chang, J.; Yan, N. Electrochemical Detection of Biogenic Amines During Food Spoilage Using an Integrated Sensing RFID Tag. *Sens. Actuators, B* **2014**, *202*, 1298–1304.
25. Potyrailo, R. A.; Burns, A.; Surman, C.; Lee, D. J.; McGinniss, E. Multivariable Passive RFID Vapor Sensors: Roll-to-Roll Fabrication on a Flexible Substrate. *Analyst* **2012**, *137*, 2777–2781.
26. Yoon, H.; Xie, J.; Abraham, J. K.; Varadan, V. K.; Ruffin, P. B. Passive Wireless Sensors Using Electrical Transition of Carbon Nanotube Junctions in Polymer Matrix. *Smart Mater. Struct.* **2006**, *15*, S14–S20.
27. Fiddes, L. K.; Yan, N. RFID Tags for Wireless Electrochemical Detection of Volatile Chemicals. *Sens. Actuators, B* **2013**, *186*, 817–823.
28. Manzari, S.; Catini, A.; Pomarico, G.; Natale, C. D.; Marrocco, G. Development of an UHF RFID Chemical Sensor Array for Battery-Less Ambient Sensing. *IEEE Sens. J.* **2014**, *14*, 3616–3623.
29. Koski, K.; Koski, E.; Virtanen, J.; Bjorninen, T.; Sydanheimo, L.; Ukkonen, L.; Elsherbeni, A. Z. Inkjet-Printed Passive UHF RFID Tags: Review and Performance Evaluation. *Int. J. Adv. Des. Manuf. Technol.* **2012**, *62*, 167–182.
30. Virtanen, J.; Yang, F.; Ukkonen, L.; Elsherbeni, A. Z.; Babar, A. A.; Sydanheimo, S. Dual Port Temperature Sensor Tag for Passive UHF RFID Systems. *Chem. Rev.* **2014**, *34*, 154–169.
31. Buffi, A.; Nepa, P.; Lombardini, F. A Phase-Based Technique for Localization of UHF-RFID Tags Moving on a Conveyor Belt: Performance Analysis and Test-Case Measurements. *IEEE Sens. J.* **2015**, *15*, 387–396.
32. Merilampi, S. L.; Virkki, J.; Ukkonen, L.; Sydanheimo, L. Testing the Effects of Temperature and Humidity on Printed Passive UHF RFID Tags on Paper Substrate. *Int. J. Electron.* **2014**, *101*, 711–730.
33. Chen, J.; Zhang, J.; Wang, M.; Li, Y. High-Temperature Hydrogen Sensor Based on Platinum Nanoparticle-Decorated SiC Nanowire Device. *Sens. Actuators, B* **2014**, *201*, 402–406.
34. Ma, X.; Zhao, K.; Tang, H.; Chen, Y.; Lu, C.; Liu, W.; Gao, Y.; Zhao, H.; Tang, Z. New Insight into the Role of Gold Nanoparticles in Au@CdS Core−Shell Nanostructures for Hydrogen Evolution. *Small* **2014**, *10*, 4664–4670.
35. Li, X.; Liu, Y.; Hemminger, J. C.; Penner, R. M. Catalytically Activated Palladium@Platinum Nanowires for Accelerated Hydrogen Gas Detection. *ACS Nano* **2015**, *9*, 3215–3225.
36. Yin, Z.; Chen, B.; Bosman, M.; Cao, X.; Chen, J.; Zheng, B.; Zhang, H. Au Nanoparticle-Modified MoS_2 Nanosheet-Based Photoelectrochemical Cells for Water Splitting. *Small* **2014**, *10*, 3537–3543.
37. Ngene, P.; Radeva, T.; Slaman, M.; Westerwaal, R. J.; Schreuders, H.; Dam, B. Seeing Hydrogen in Colors: Low-Cost and Highly Sensitive Eye Readable Hydrogen Detectors. *Adv. Funct. Mater.* **2014**, *24*, 2374–2382.
38. Liu, B.; Cai, D.; Liu, Y.; Li, H.; Weng, C.; Zeng, G.; Li, Q.; Wang, T. High-Performance Room-Temperature Hydrogen Sensors Based on Combined Effects of Pd Decoration and Schottky Barriers. *Nanoscale* **2013**, *5*, 2505–2510.
39. Zhu, L.; Jia, Y.; Gai, G.; Ji, S.; Luo, J.; Yao, Y. Ambipolarity of Large-Area Pt-Functionalized Graphene Observed in H_2 Sensing. *Sens. Actuators, B* **2014**, *190*, 134–140.
40. Tsukada, K.; Kiwa, T.; Yamaguchi, T.; Migitaka, S.; Goto, Y.; Yokosawa, K. A Study of Fast Response Characteristics for Hydrogen Sensing with Platinum FET Sensor. *Sens. Actuators, B* **2006**, *114*, 158–163.
41. Kaniyoor, A.; Jafri, R. I.; Arockiadoss, T.; Ramaprabhu, S. Nanostructured Pt Decorated Graphene and Multi Walled Carbon nanotube Based Room Temperature Hydrogen Gas Sensor. *Nanoscale* **2009**, *1*, 382–386.
42. Kundu, P.; Nethravathi, C.; Deshpande, P. A.; Rajamathi, M.; Madras, G.; Ravishankar, N. Ultrafast Microwave-Assisted Route to Surfactant-Free Ultrafine Pt Nanoparticles on Graphene: Synergistic Co-reduction Mechanism and High Catalytic Activity. *Chem. Mater.* **2011**, *23*, 2772–2780.
43. Si, Y.; Samulski, E. T. Exfoliated Graphene Separated by Platinum Nanoparticles. *Chem. Mater.* **2008**, *20*, 6792–6797.
44. Wang, Z.; Li, F.; Xia, J.; Xia, L.; Zhang, F.; Bi, S.; Shi, G.; Xia, Y.; Liu, J.; Li, Y.; et al. An Ionic Liquid-Modified Graphene Based Molecular Imprinting Electrochemical Sensor for Sensitive Detection of Bovine Hemoglobin. *Biosens. Bioelectron.* **2014**, *61*, 391–396.
45. Cao, Z.; Wang, P.; Gao, W.; Tao, L.; Suk, J. W.; Rouff, R. S.; Akinwande, D.; Huang, R.; Liechti, K. M. A Blister Test for Interfacial Adhesion of Large-Scale Transferred Graphene. *Carbon* **2014**, *69*, 390–400.
46. Favier, F.; Walter, E. C.; Zach, M. P.; Benter, T.; Penner, R. M. Hydrogen Sensors and Switched from Electrodeposited Palladium Mesowire Arrays. *Science* **2001**, *293*, 2227–2231.
47. Zeng, X. Q.; Latimer, M. L.; Xiao, Z. L.; Panuganti, S.; Welp, U.; Kwok, W. K.; Xu, T. Hydrogen Gas Sensing with Networks of Ultrasmall Palladium Nanowires Formed on Filtration Membranes. *Nano Lett.* **2011**, *11*, 262–268.